Turbo-Alternator Stalling Protection Using Available-Power Estimate

Taylor T. Johnson
Electrical and Computer Engineering
University of Illinois at Urbana-Champaign
Urbana, IL 61801
Email: johnso99@illinois.edu

Albert E. Hoefel
Schlumberger Technology Corporation
Sugar Land, TX 77843
Email: hoefel1@slb.com

***Abstract*—In environments where electromechanical loads may suffer from disturbances with large magnitude—such as in sampling downhole reservoirs—stalling protection for the power source of the alternator may be critical to prevent potentially catastrophic system failure. First, a real-time estimation method is described to determine the maximum available electrical power produced by a turbo-alternator for a given volumetric flow rate acting on the turbine. Next, the available-power estimate and used electrical power measurement are used to prevent turbine stalling by regulating an electromechanical load—in this case a permanent magnet synchronous motor (PMSM)—to draw less power. The stalling protection is implemented through an additional proportional-integral-derivative (PID) controller for load power, which is cascaded outside already cascaded velocity and torque PID controllers used for control of the PMSM. To ensure fast tracking, the power PID controller implements integral anti-windup. An experimental evaluation of the methodology is presented.**

***Index Terms*—adaptive control, alternator, system identification, turbine, turbo-alternator, stalling**

I. Introduction

Turbo-alternator stalling and subsequent loss or decrease of electrical power could produce countless faults, from full system power reset to unstable—or at least uncharacterized—plant regulation. Stalling can occur if the electromechanical *load power* required, P_L, is too large a fraction of the turbo-alternator's *maximum available power*, P_{max}, which is the maximum power the turbine can provide for a given volumetric flow rate Q. Physically, stalling for a turbo-alternator means that the turbine is not receiving enough power from the fluid flow driving it, thus the flow Q turning the turbine is too small to spin the alternator fast enough to keep up with the power demands. This P_{max} corresponds to the maxima of each of the three parabolas in the power-versus-angular velocity plots in Fig. 1, which are distinct for three flow rates $Q_1 > Q_2 > Q_3$. As flow rate increases, there is roughly a cubic increase in P_{max}. This paper describes a method to prevent turbo-alternator stalling by regulating the load power, P_L, if it becomes near the maximum available power, P_{max}.

Unfortunately, in many systems, such as ours, the flow rate Q is unobservable. Thus the first problem is system identification [1], and geometrically we must determine the parameters describing parabolas like those in Fig. 1. The system identification problem, for an unknown volumetric flow rate Q, a given *load angular velocity* measurement ω_L—the velocity with which the alternator spins for some load—, and a given used power measurement P_L, is to determine an estimate $\hat{P}_{max}$ of P_{max}. Additionally, an estimate $\hat{\omega}_f$ of alternator *free-spin angular velocity* ω_f is necessary to describe the parabolas in Fig. 1, where ω_f is the velocity the alternator would spin at under no load. A point (ω_L, P_L) in Fig. 1 lies on the parabola defined by the flow rate Q, so for a fixed flow rate Q, a parabola is defined with a particular P_{max} and ω_f, and the point (ω_L, P_L) will travel along this parabola for varying electromechanical loads. However, to complicate matters further, Q is time-varying, so the parabola changes over time and thus a real-time estimation method is necessary.

The turbine is *stalling* for load power P_L if $\omega_L \leq \frac{\omega_f}{2}$, that is, if the point (ω_L, P_L) lies to the left of the midpoint of the parabola, $(\frac{\omega_f}{2}, P_{max})$, as shown by the stalling region shaded for the black curve in Fig. 1. Intuitively, the regulation problem

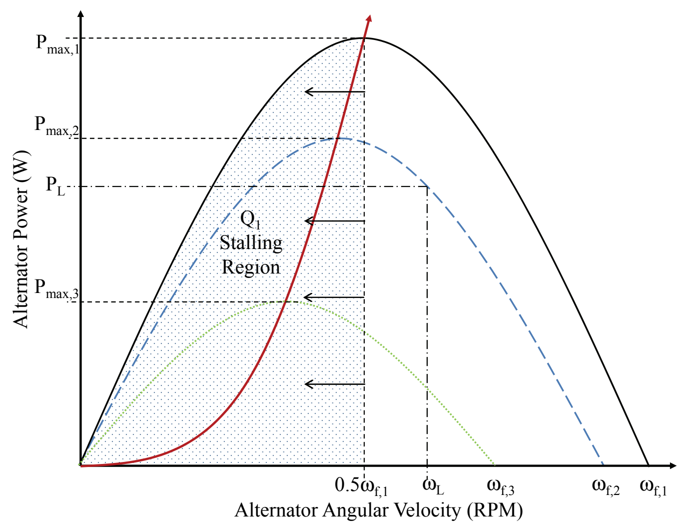

Fig. 1. Geometric problem description and cubic maximum power growth for three flow rates, $Q_1 > Q_2 > Q_3$, where Q_1 corresponds to the black curve, Q_2 to the blue dashed one, and Q_3 to the green dotted one.

This work was completed while the first author was employed as an intern by Schlumberger during summer 2010.

to prevent stalling is to ensure that the point (ω_L, P_L) lies on the right half of the parabola. Given an estimate $\hat{P}_{max}$, the second problem is to regulate the electromechanical load power P_L to be at most some $0 < \rho < 1$ percentage of available power (that is, ensure $P_L \leq \rho P_{max}$), assuming that $\hat{P}_{max} \approx P_{max}$. A proportional-integral-derivative (PID) controller regulates the load power P_L drawn by the permanent magnet synchronous motor (PMSM) and its load to ensure $P_L \leq \rho \hat{P}_{max}$, and additionally integral anti-windup is used to ensure that when not actively regulating P_L, the integral error does not accumulate. Assuming ω_L initially is larger than half ω_f—which is reasonable when initializing the system under low or no load—the regulation problem is to ensure P_L does not come too close to the maxima. This high-level estimation and regulation scheme is described in Fig. 2.

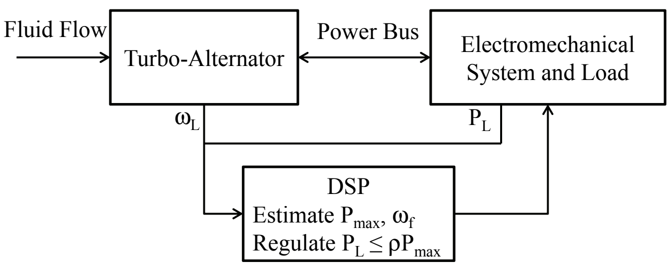

Fig. 2. High-level regulation problem

II. System Identification and Power Regulation

The system (parameter) identification problem is to estimate, for an unknown flow rate Q, 1) the maximum available power the alternator may produce P_{max} and 2) the alternator free-spin angular velocity ω_f, which is the velocity with which the alternator spins with no load. Note that we work in a discrete-time framework in which time steps are indexed by k, so a variable $x[k]$ represents the (potentially vector) value of variable x at time k, and the index k is dropped when clear. Because of real-time performance requirements, exact convergence is not required, and some small ε error from the actual parameter values is tolerable, such that $\hat{P}_{max}[k] \approx P_{max}[k]$ and $\hat{\omega}_f[k] \approx \omega_f[k]$ for all times k.

The general identification problem given an observed variable $y[k]$ is,

$$\begin{aligned} y[k] =& \phi_1[k]\theta_1^0 + \phi_2[k]\theta_2^0 + \ldots + \phi_n[k]\theta_n^0 && (1) \\ =& \phi^T[k]\theta^0, && (2) \end{aligned}$$

where $\phi^T[k] = \phi_1[k]$, $\phi_2[k]$, $\ldots$, $\phi_n[k]$ are called the *regression variables* and are known functions (such as measurements) that may depend on other known variables, determine the initial *model parameters* $\theta^0 = \theta_1^0$, θ_2^0, $\ldots$, θ_n^0. Only estimates $\hat{\theta}$ of θ^0 will be attainable, so at time step k, the estimation error is

$$e[k] = y[k] - \phi^T[k]\hat{\theta}[k].$$

We begin with the particular system model we are working with, the downhole turbo-alternator powered by drilling fluid flow. For this system, the nonlinear problem is to solve the vector-valued function $(P_{max}[k], \omega_f[k]) = f(P_L[k], \omega_L[k], \omega_L[k-1])$, where

$$\begin{aligned} y[k] =& P_L[k] \\ =& \phi^T[k]\hat{\theta}[k] \\ =& \frac{4P_{max}[k]}{\omega_f[k]}\omega_L[k] - \left(\frac{4P_{max}[k]}{\omega_f[k]^2} + \frac{J[k]}{2T_s}\right)\omega_L[k]^2 \\ &+ \frac{J[k]}{2T_s}\omega_L[k-1]^2, && (3) \end{aligned}$$

$$\phi[k] = \left(\omega_L[k], \omega_L[k]^2, \omega_L[k-1]^2\right)^T, \text{ and} \quad (4)$$

$$\hat{\theta}[k] = \left(\frac{4P_{max}[k]}{\omega_f[k]}, -\left(\frac{4P_{max}[k]}{\omega_f[k]^2} + \frac{J[k]}{2T_s}\right), \frac{J[k]}{2T_s}\right)^T, \quad (5)$$

where all variables except the sampling time T_s and inertia J have been introduced, and the exponent T denotes the transpose. An approximation of turbine power is

$$P_L = P_{max} - \frac{4P_{max}}{\omega_f^2}(\omega_L - \frac{\omega_f}{2})^2.$$

The first estimation method is simple interpolation using a cubic curve fit of the alternator measured speed $\omega_L[k]$ to estimate alternator maximum available power $\hat{P}_{max}[k]$. The curve being fit is the red one in Fig. 1, which passes through P_{max} and is roughly cubic in ω_L. The interpolation method is simply

$$\hat{P}_{max}[k] = a_3\omega_L[k]^3 + a_2\omega_L[k]^2 + a_1\omega_L[k] + a_0,$$

where the a_i coefficients are the parameters of a cubic fit to the red line in Fig. 1.

Interpolation is always accurate in an absolute sense; that is, the value it determines cannot diverge. However it likewise cannot converge, resulting in steady-state error. The usefulness of this method is thus to seed initial estimates for more sophisticated methods which do converge, which may require initialization to a value near the extrema [2].

From the interpolated estimate $\hat{P}_{max}[k]$ and the known quantities, the free-spin $\hat{\omega}_f[k]$ and inertia $\hat{J}[k]$ are determined as

$$\hat{\omega}_f[k] = \frac{2\omega_L[k]}{\sqrt{1 - \frac{P_L[k]}{\hat{P}_{max}[k]}} + 1}, \text{ and} \quad (6)$$

$$\hat{J}[k] = \frac{8\hat{P}_{max}[k]\omega_L[k]\left(\hat{\omega}_f[k] - \omega_L[k]\right)}{\hat{\omega}_f^2\left(\omega_L^2[k] - \omega_L^2[k-1]\right)}. \quad (7)$$

These quantities are finally transformed to yield approximations of the estimation variables, $\hat{\theta}[k]$, as

$$\hat{\theta}_0[k] = \frac{4P_{max}[k]}{\omega_f[k]}, \quad (8)$$

$$\hat{\theta}_1[k] = -\frac{\hat{\theta}_0[k]}{\omega_f[k]} - \frac{J[k]}{2}, \text{ and} \quad (9)$$

$$\hat{\theta}_2[k] = \frac{J[k]}{2}, \quad (10)$$

where $\hat{\theta}_i[k]$ is the i^{th} entry of the vector $\hat{\theta}$ at time step k.

The second estimation method is recursive least squares (RLS) [1], and is initialized with $\hat{\theta}$ defined in (8), (9), and (10). The RLS algorithm with exponential forgetting is described as

$$\hat{\theta}[k] = \hat{\theta}[k-1] + K[k]\left(y[k] - \phi[k]^T\hat{\theta}[k-1]\right), \tag{11}$$

$$K[k] = P[k-1]\phi[k]\left(\lambda + \phi[k]^T P[k-1]\phi[k]\right)^{-1}, \text{ and} \tag{12}$$

$$P[k] = \frac{1}{\lambda}\left(I - K[k]\phi^T[k]\right)P[k-1], \tag{13}$$

where P is called the inverse correlation matrix, K is the gain, and $\lambda = e^{-h/T_f}$ is the forgetting factor, where h is the sampling period and T_f is the time constant for exponential forgetting. RLS with exponential forgetting performs a least-squares fit on a finite number of past data samples [3]. The alternator model above is nonlinear. However, it is possible to use the RLS algorithm on nonlinear models if the output y can be written linearly in terms of measured variables ϕ and estimated quantities $\hat{\theta}$, which is the case as shown in (3), (4), and (5). The desired unknowns can then be solved for as

$$\hat{\omega}_f[k] = -\frac{\hat{\theta}_0[k]}{\hat{\theta}_1[k] + \hat{\theta}_2[k]}, \text{ and} \tag{14}$$

$$\hat{P}_{max}[k] = \frac{\omega_f[k]\hat{\theta}_0[k]}{4}. \tag{15}$$

Under suitable assumptions (see, for instance [1]), the RLS method ensures convergence of $\hat{\theta}[k]$ to θ^0 as $k \to \infty$. This means that with the previous transformation of $\hat{\theta}[k]$ to $\hat{P}_{max}[k]$ and $\hat{\omega}_f[k]$ in (15) and (14) respectively, that for any error $\varepsilon > 0$, $\exists N > 0$ such that $\left|\hat{P}_{max}[N] - P_{max}[N]\right| < \varepsilon$. Thus, it is reasonable to assume that for a sufficiently large k, $\hat{P}_{max}[k] \approx P_{max}[k]$.

Power Regulation: Given $\hat{P}_{max}[k]$ and assuming $\hat{P}_{max}[k] \approx P_{max}[k]$, the regulation problem is to ensure that the power consumed by the system, $P_L[k]$—primarily the PMSM and its load, but also various power electronics—does not exceed some ρ fraction of $\hat{P}_{max}[k]$, guaranteeing $P_L[k] \le \rho\hat{P}_{max}[k]$ for all time k. Complications may arise from the electromechanical load, which like the flow rate, may also experience time-varying disturbances. The PMSM is in a three-phase Y-configuration. The PMSM is controlled with cascaded velocity and torque PIDs as shown in Fig. 3. While not completely indicated in the figure for simplicity of presentation, it is controlled using standard field-oriented control [4] and eventually pulse-width modulation (PWM). In Fig. 3 we have shown the alternator load angular velocity ω_L as being an output of the PMSM, but this was in part for presentation. In actuality, ω_L is a measurement from the alternator as described above for the estimation, but is also a function of the load on the PMSM, since as the load varies, ω_L will also vary by traveling along a given parabola as described earlier in Fig. 1.

We have not indicated the load in the diagram, but it is a pump interacting with the outside environment and is subject to disturbance. Because of the disturbances, the load on the pump may require anywhere from a small fraction of available power, to a large fraction of available power (or potentially all available power, which could induce a stall).

A PID was added as shown in Fig. 3 to regulate power $P_L \le \rho\hat{P}_{max}$, and the output of this PID is then used as an input

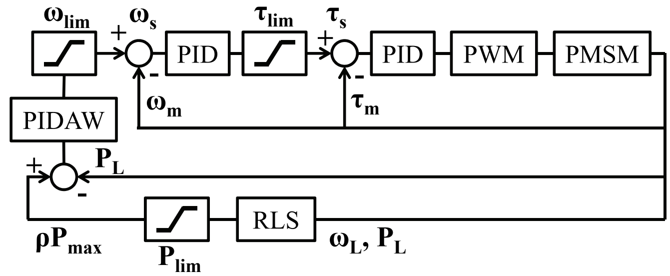

Fig. 3. PMSM control loop, where ω_{lim} indicates the limiter for motor speed, τ_{lim} is the limiter for motor torque, P_{lim} is the limiter for available power, ω_s is the PMSM velocity set-point, ω_m is the PMSM velocity measurement, τ_m is the PMSM torque measurement, τ_s is the PMSM torque set-point, the RLS block represents the estimation scheme previously described, and the PIDAW block represents the power PID controller with anti-windup.

to the velocity PID via the speed limiter ω_{lim}. Standard PID regulation can ensure $P_L = \rho\hat{P}_{max}[k]$ if $P_L \ge \rho\hat{P}_{max}[k]$, but if the system is consuming power such that $P_L[k] < \rho\hat{P}_{max}[k]$, then no regulation is necessary. With a standard PID implementation, however, integral error may accumulate, so our PID includes integral anti-windup. Essentially, when not regulating, the integral term for power regulation is ignored, and the PMSM velocity set-point ω_s is used instead.

III. Experimental Setup and Results

The experimental setup is shown in Fig. 4, where another PMSM is configured to drive the alternator and serve as a flow-rate simulator. Rather than using an actual volumetric fluid flow Q, as shown in Fig. 4, an additional PMSM was configured as a *flow rate simulator* to drive the alternator at speeds corresponding to time-varying flow rates $Q[k]$ with power $P_Q[k] = P_m[k]$. A simple National Instruments LabWindows/CVI program was written to interface with the motor controller of the flow-simulator PMSM; particularly, the program reads a speed provided by the PMSM resolver, then generates the desired torque command corresponding to the desired flow rate. The system identification and PID controllers for the load PMSM are implemented on a digital signal processor (DSP) as indicated in Fig. 4. Using the speed measurement from a resolver interfaced with the PMSM, along with a given desired flow rate to simulate, a torque was calculated to drive the motor along the corresponding power parabola, like those in Fig. 1.

In downhole drilling scenarios, *mud-pulse telemetry* is used to communicate with downhole computers via *downlinks* by encoding a rectangular pulse train on top of the normal drilling fluid flow Q, resulting in a decrease of Q's magnitude by 5% to 25%, creating a time-varying flow-rate $Q[k]$. During a downlink, the total flow rate typically ranges between 300 gallons per minute (GPM) and 600 GPM, with 400 GPM being the most common. For instance, assuming the flow rate is 400 GPM, the downlink may vary the flow rate down to between 300 to 380 GPM. Observe that the high side of a downlink, say at 400 GPM, may satisfy $P_L[k] < \rho\hat{P}_{max}[k]$, but the low side of the downlink may not, where, for instance, at

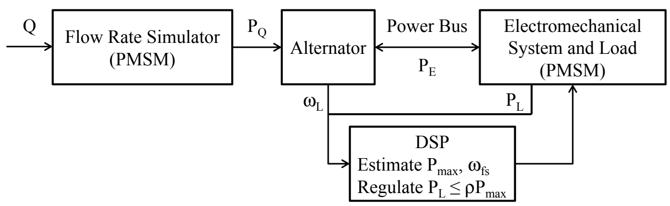

Fig. 4. Experimental setup

300 GPM, $P_L[k] > \rho\hat{P}_{max}[k]$, which could induce a stall. For fast tracking, even if the power PID is not regulating, error accumulation (integral windup) must not occur when P_L is not reaching the desired output of the power PID, as regulation may be necessary at the next time instant due to variation in Q, which can decrease P_{max} and cause $P_L \geq \rho\hat{P}_{max}$. The flow-rate simulator was then configured to simulate this downhole mud-pulse telemetry by varying the flow-rate magnitude.

Without anti-windup, experiments showed the power regulator had to decrement the large integral error term that had accumulated due to not regulating for a long period, resulting in slow power tracking and an inability to prevent stalling. All below experiments show time steps corresponding to the discrete time steps k from earlier, which have a period of 62.5 milliseconds. Also, notice that the occasional, roughly periodic large drops in used power $P_L[k]$ in several plots below are due to load variation (in particular, the load PMSM reversing).

Fig. 5 illustrates power regulation while varying ρ such that at different times more or less than ρ of $\hat{P}_m$ is desired. For stalling protection, ρ would be chosen *a priori*, and the comparison to ρ is done by defining the actual ratio achieved,

$$\rho_a \triangleq \frac{P_L[k]}{\hat{P}_m[k]}. \tag{16}$$

This plot shows that the method can handle varying flow rates and load variations when the load power requirement is such that at some times P_L requires regulation, but at other times does not.

Fig. 6 illustrates the anti-windup and fast regulation to prevent stalling when the low side of the downlink at 300 GPM yields P_m such that $P_L > \rho\hat{P}_m$ while at 325 GPM, regulation is not needed since $P_L \leq \rho\hat{P}_m$. Note how quickly the power PID regulates P_L upon a high-to-low flow-rate transition (for instance, see ρ_a at about time steps 1299 and 2833), which is what is needed for stalling protection. Note that some drops in P_L are due to the time-varying electromechanical load. Thus, Fig. 6 illustrate that the power PID achieves reasonable tracking and avoids integral windup.

Finally, we illustrate an example of actual stalling protection in Figs. 7 and 8 using choices of $\rho = 0.8$ and $\rho = 0.85$, respectively, which were empirically determined. For the remaining plots, the square-wave downlink simulation had a period of 16 seconds. The load was again configured to illustrate anti-windup, that is, the load is such that the high side of the downlink simulating 330 GPM does not require power regulation, whereas the low side at 300 GPM does require

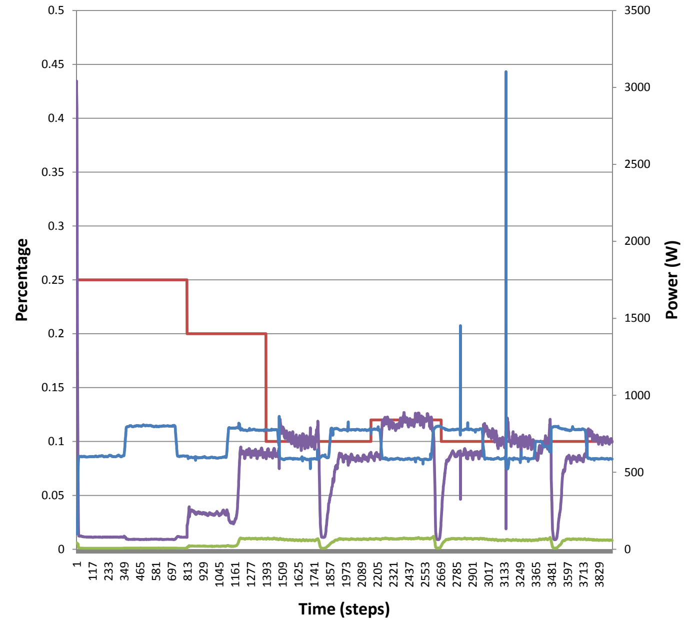

Fig. 5. Power regulation from 240 GPM to 270 GPM, where ρ is in red, ρ_a in purple, $\hat{P}_m$ in blue, and P_L in green.

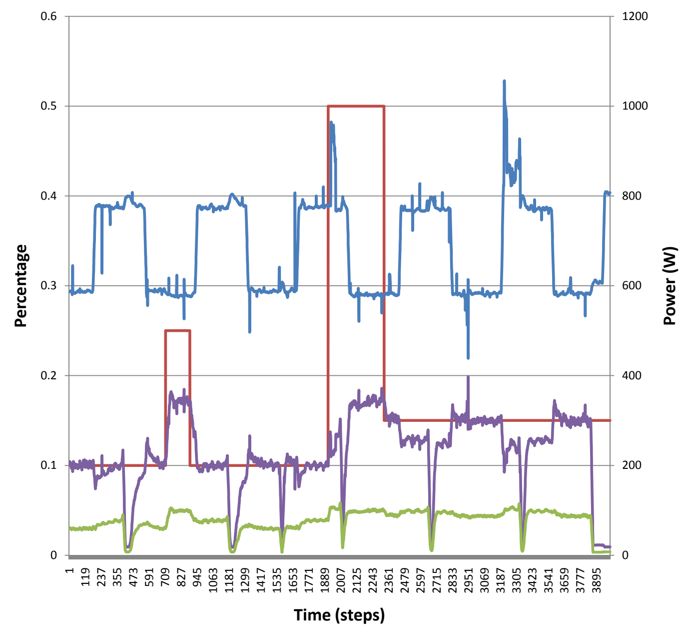

Fig. 6. Power regulation from 300 GPM to 325 GPM, where ρ is in red, ρ_a in purple, $\hat{P}_m$ in blue, and P_L in green.

regulation. During a stall, potentially uncontrolled operation of the system can occur because, as the turbine slows, alternator output voltage will drop, causing a cascade of power losses to different subsystems, such as the electromechanical load being regulated. Because of the interaction of the cascaded control loops, a stall is not catastrophic in this system, but instead induces oscillations on the load, because the load increases with PMSM speed, as seen by the red line in Fig. 9, which is the rectified alternator voltage in a stall. In Fig. 9, the red line

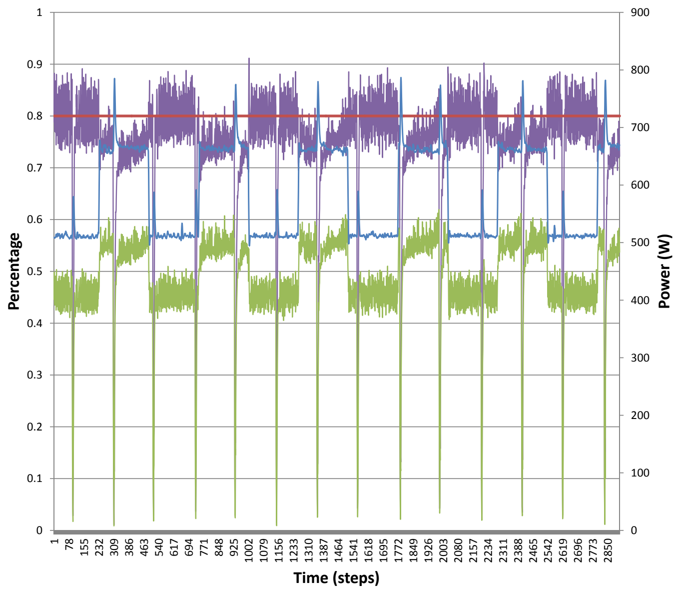

Fig. 7. Stalling protection for ρ = 0.80 with downlink from 300 GPM to 330 GPM, where ρ is in red, ρ_a in purple, $\hat{P}_m$ in blue, and P_L in green.

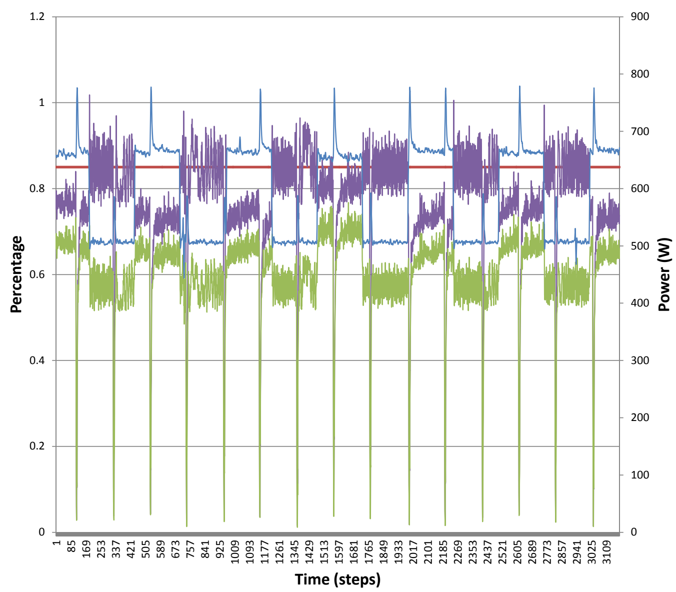

Fig. 8. Stalling protection for ρ = 0.85 with downlink from 300 GPM to 330 GPM, where ρ is in red, ρ_a in purple, $\hat{P}_m$ in blue, and P_L in green.

shows the alternator voltage for ρ = 0.95, which oscillates as the turbine simulator cannot provide enough power on the low side of a downlink. This is also clearly seen between time steps 371 and 704 in the power plot of Fig. 10, which corresponds to the same experiment. Thus, because of load fluctuations, ρ = 0.95 does not prevent stalling, so we settled on a lower value.

IV. Conclusions and Future Work

This paper presented a system identification method to estimate the maximum available power a turbo-alternator produces for some unknown volumetric flow rate, and then uses

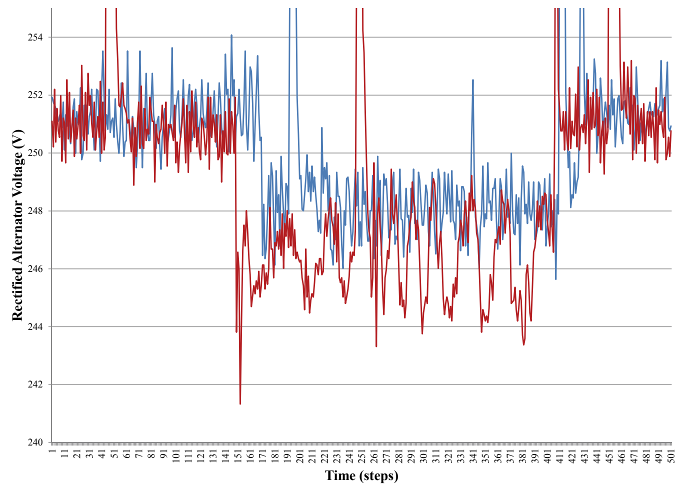

Fig. 9. Rectified alternator voltage with stalling protection for ρ = 80 in blue and without stalling protection for ρ = 0.95 in red.

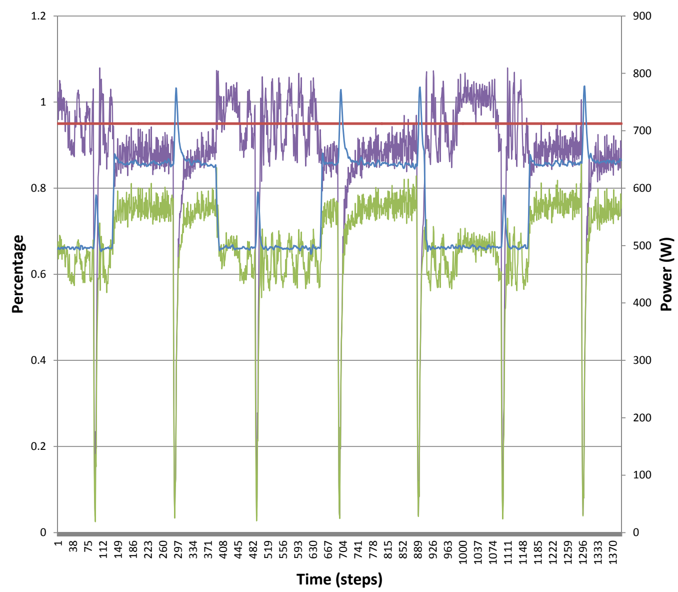

Fig. 10. Stall due to too high choice of ρ at 0.95, with downlink from 300 GPM to 330 GPM, where ρ is in red, ρ_a in purple, $\hat{P}_m$ in blue, and P_L in green.

this estimate in stalling prevention. To ensure robustness, the method described in this paper should be tested in a real flow loop, rather than simulated in the experimental setup described in Fig. 4. Modern methods for varying the forgetting factor of the RLS algorithm from the literature could be employed to see if they improve tracking performance (see for instance, [3]). We could see try to improve estimation by either using more special-purpose least-squares algorithms such as [5], [6], [7] or a nonlinear formulation of the problem [8] with higher-order terms of the alternator plant model. While not reported here, we performed a limited study of numerical stability of our implementation of the recursive methods, but more work is needed [9]. A formalized stability analysis of the interaction of the various saturations and the anti-windup would be interesting, perhaps using the tools of [10], [11], and we could perhaps improve our anti-windup technique using [12].

Acknowledgements

We wish to acknowledge the support of the other engineers, lab technicians, and interns at Schlumberger which helped make this work possible, particularly Robert Champlin, Shayan Darayan, William Do, Toshi Fujinawa, Kent Harms, Tuan Hoang, Ronnie Meyers, and Steven Villareal.

References

[1] K. J. Åström and B. Wittenmark, *Adaptive Control*, 2nd ed. Reading, MA: Addison-Wesley Publishing Company, 1995.

[2] I. Griva, S. G. Nash, and A. Sofer, *Linear and Nonlinear Optimization*, 2nd ed. Philadelphia, PA: Society for Industrial and Applied Mathematics, 2009.

[3] S. Ciochina, C. Paleologu, J. Benesty, and A. Enescu, "On the influence of the forgetting factor of the rls adaptive filter in system identification," in *Signals, Circuits and Systems, 2009. ISSCS 2009. International Symposium on*, Jul. 2009, pp. 1–4.

[4] P. Vas, *Sensorless Vector and Direct Torque Control*. Oxford University Press, 1998.

[5] I. D. Coope, "Circle fitting by linear and nonlinear least squares," *J. Optim. Theory Appl.*, vol. 76, no. 2, pp. 381–388, 1993.

[6] A. Fitzgibbon, M. Pilu, and R. B. Fisher, "Direct least square fitting of ellipses," *IEEE Trans. Pattern Anal. Mach. Intell.*, vol. 21, no. 5, pp. 476–480, 1999.

[7] N. Chernov and C. Lesort, "Least squares fitting of circles," *J. Math. Imaging Vis.*, vol. 23, no. 3, pp. 239–252, 2005.

[8] J. E. Dennis, Jr., D. M. Gay, and R. E. Walsh, "An adaptive nonlinear least-squares algorithm," *ACM Trans. Math. Softw.*, vol. 7, no. 3, pp. 348–368, 1981.

[9] D. Slock and T. Kailath, "Numerically stable fast transversal filters for recursive least squares adaptive filtering," *Signal Processing, IEEE Transactions on*, vol. 39, no. 1, pp. 92–114, Jan. 1991.

[10] M. V. Kothare, P. J. Campo, M. Morari, and C. N. Nett, "A unified framework for the study of anti-windup designs," *Automatica*, vol. 30, no. 12, pp. 1869–1883, 1994.

[11] C. Edwards and I. Postlethwaite, "Anti-windup and bumpless-transfer schemes," *Automatica*, vol. 34, no. 2, pp. 199–210, 1998.

[12] S. Sajjadi-Kia and F. Jabbari, "Modified anti-windup compensators for stable plants," *Automatic Control, IEEE Transactions on*, vol. 54, no. 8, pp. 1934–1939, Aug. 2009.